Editors' Suggestion

Search for Neutrino-Induced Neutral-Current Δ Radiative Decay in MicroBooNE and a First Test of the MiniBooNE Low Energy Excess under a Single-Photon Hypothesis

P. Abratenko,[33] R. An,[14] J. Anthony,[4] L. Arellano,[18] J. Asaadi,[32] A. Ashkenazi,[30] S. Balasubramanian,[11] B. Baller,[11] C. Barnes,[20] G. Barr,[23] V. Basque,[18] L. Bathe-Peters,[13] O. Benevides Rodrigues,[29] S. Berkman,[11] A. Bhanderi,[18] A. Bhat,[29] M. Bishai,[2] A. Blake,[16] T. Bolton,[15] J. Y. Book,[13] L. Camilleri,[9] D. Caratelli,[11] I. Caro Terrazas,[8] R. Castillo Fernandez,[11] F. Cavanna,[11] G. Cerati,[11] Y. Chen,[1] D. Cianci,[9] J. M. Conrad,[19] M. Convery,[26] L. Cooper-Troendle,[36] J. I. Crespo-Anadón,[5] M. Del Tutto,[11] S. R. Dennis,[4] P. Detje,[4] A. Devitt,[16] R. Diurba,[21] R. Dorrill,[14] K. Duffy,[11] S. Dytman,[24] B. Eberly,[28] A. Ereditato,[1] J. J. Evans,[18] R. Fine,[17] G. A. Fiorentini Aguirre,[27] R. S. Fitzpatrick,[20] B. T. Fleming,[36] N. Foppiani,[13] D. Franco,[36] A. P. Furmanski,[21] D. Garcia-Gamez,[12] S. Gardiner,[11] G. Ge,[9] S. Gollapinni,[31,17] O. Goodwin,[18] E. Gramellini,[11] P. Green,[18] H. Greenlee,[11] W. Gu,[2] R. Guenette,[13] P. Guzowski,[18] L. Hagaman,[36] O. Hen,[19] C. Hilgenberg,[21] G. A. Horton-Smith,[15] A. Hourlier,[19] R. Itay,[26] C. James,[11] X. Ji,[2] L. Jiang,[34] J. H. Jo,[36] R. A. Johnson,[7] Y.-J. Jwa,[9] D. Kalra,[9] N. Kamp,[19] N. Kaneshige,[3] G. Karagiorgi,[9] W. Ketchum,[11] M. Kirby,[11] T. Kobilarcik,[11] I. Kreslo,[1] R. LaZur,[8] I. Lepetic,[25] K. Li,[36] Y. Li,[2] K. Lin,[17] B. R. Littlejohn,[14] W. C. Louis,[17] X. Luo,[3] K. Manivannan,[29] C. Mariani,[34] D. Marsden,[18] J. Marshall,[35] D. A. Martinez Caicedo,[27] K. Mason,[33] A. Mastbaum,[25] N. McConkey,[18] V. Meddage,[15] T. Mettler,[1] K. Miller,[6] J. Mills,[33] K. Mistry,[18] A. Mogan,[31] T. Mohayai,[11] J. Moon,[19] M. Mooney,[8] A. F. Moor,[4] C. D. Moore,[11] L. Mora Lepin,[18] J. Mousseau,[20] M. Murphy,[34] R. Murrells,[18] D. Naples,[24] A. Navrer-Agasson,[18] M. Nebot-Guinot,[10] R. K. Neely,[15] D. A. Newmark,[17] J. Nowak,[16] M. Nunes,[29] O. Palamara,[11] V. Paolone,[24] A. Papadopoulou,[19] V. Papavassiliou,[22] S. F. Pate,[22] N. Patel,[16] A. Paudel,[15] Z. Pavlovic,[11] E. Piasetzky,[30] I. D. Ponce-Pinto,[36] S. Prince,[13] X. Qian,[2] J. L. Raaf,[11] V. Radeka,[2] A. Rafique,[15] M. Reggiani-Guzzo,[18] L. Ren,[22] L. C. J. Rice,[24] L. Rochester,[26] J. Rodriguez Rondon,[27] M. Rosenberg,[24] M. Ross-Lonergan,[9] G. Scanavini,[36] D. W. Schmitz,[6] A. Schukraft,[11] W. Seligman,[9] M. H. Shaevitz,[9] R. Sharankova,[33] J. Shi,[4] J. Sinclair,[1] A. Smith,[4] E. L. Snider,[11] M. Soderberg,[29] S. Söldner-Rembold,[18] P. Spentzouris,[11] J. Spitz,[20] M. Stancari,[11] J. St. John,[11] T. Strauss,[11] K. Sutton,[9] S. Sword-Fehlberg,[22] A. M. Szelc,[10] W. Tang,[31] K. Terao,[26] C. Thorpe,[16] D. Totani,[3] M. Toups,[11] Y.-T. Tsai,[26] M. A. Uchida,[4] T. Usher,[26] W. Van De Pontseele,[23,13] B. Viren,[2] M. Weber,[1] H. Wei,[2] Z. Williams,[32] S. Wolbers,[11] T. Wongjirad,[33] M. Wospakrik,[11] K. Wresilo,[4] N. Wright,[19] W. Wu,[11] E. Yandel,[3] T. Yang,[11] G. Yarbrough,[31] L. E. Yates,[19] H. W. Yu,[2] G. P. Zeller,[11] J. Zennamo,[11] and C. Zhang[2]

(MicroBooNE Collaboration)[*]

[1]*Universität Bern, Bern CH-3012, Switzerland*
[2]*Brookhaven National Laboratory (BNL), Upton, New York 11973, USA*
[3]*University of California, Santa Barbara, California 93106, USA*
[4]*University of Cambridge, Cambridge CB3 0HE, United Kingdom*
[5]*Centro de Investigaciones Energéticas, Medioambientales y Tecnológicas (CIEMAT), Madrid E-28040, Spain*
[6]*University of Chicago, Chicago, Illinois 60637, USA*
[7]*University of Cincinnati, Cincinnati, Ohio 45221, USA*
[8]*Colorado State University, Fort Collins, Colorado 80523, USA*
[9]*Columbia University, New York, New York 10027, USA*
[10]*University of Edinburgh, Edinburgh EH9 3FD, United Kingdom*
[11]*Fermi National Accelerator Laboratory (FNAL), Batavia, Illinois 60510, USA*
[12]*Universidad de Granada, Granada E-18071, Spain*
[13]*Harvard University, Cambridge, Massachusetts 02138, USA*
[14]*Illinois Institute of Technology (IIT), Chicago, Illinois 60616, USA*
[15]*Kansas State University (KSU), Manhattan, Kansas 66506, USA*
[16]*Lancaster University, Lancaster LA1 4YW, United Kingdom*
[17]*Los Alamos National Laboratory (LANL), Los Alamos, New Mexico 87545, USA*
[18]*The University of Manchester, Manchester M13 9PL, United Kingdom*
[19]*Massachusetts Institute of Technology (MIT), Cambridge, Massachusetts 02139, USA*
[20]*University of Michigan, Ann Arbor, Michigan 48109, USA*
[21]*University of Minnesota, Minneapolis, Minnesota 55455, USA*
[22]*New Mexico State University (NMSU), Las Cruces, New Mexico 88003, USA*
[23]*University of Oxford, Oxford OX1 3RH, United Kingdom*

[24]University of Pittsburgh, Pittsburgh, Pennsylvania 15260, USA
[25]Rutgers University, Piscataway, New Jersey 08854, USA
[26]SLAC National Accelerator Laboratory, Menlo Park, California 94025, USA
[27]South Dakota School of Mines and Technology (SDSMT), Rapid City, South Dakota 57701, USA
[28]University of Southern Maine, Portland, Maine 04104, USA
[29]Syracuse University, Syracuse, New York 13244, USA
[30]Tel Aviv University, Tel Aviv 69978, Israel
[31]University of Tennessee, Knoxville, Tennessee 37996, USA
[32]University of Texas, Arlington, Texas 76019, USA
[33]Tufts University, Medford, Massachusetts 02155, USA
[34]Center for Neutrino Physics, Virginia Tech, Blacksburg, Virginia 24061, USA
[35]University of Warwick, Coventry CV4 7AL, United Kingdom
[36]Wright Laboratory, Department of Physics, Yale University, New Haven, Connecticut 06520, USA

(Received 1 October 2021; accepted 10 February 2022; published 14 March 2022)

We report results from a search for neutrino-induced neutral current (NC) resonant $\Delta(1232)$ baryon production followed by Δ radiative decay, with a $\langle 0.8 \rangle$ GeV neutrino beam. Data corresponding to MicroBooNE's first three years of operations (6.80×10^{20} protons on target) are used to select single-photon events with one or zero protons and without charged leptons in the final state ($1\gamma 1p$ and $1\gamma 0p$, respectively). The background is constrained via an *in situ* high-purity measurement of NC π^0 events, made possible via dedicated $2\gamma 1p$ and $2\gamma 0p$ selections. A total of 16 and 153 events are observed for the $1\gamma 1p$ and $1\gamma 0p$ selections, respectively, compared to a constrained background prediction of $20.5 \pm 3.65(\text{syst})$ and $145.1 \pm 13.8(\text{syst})$ events. The data lead to a bound on an anomalous enhancement of the normalization of NC Δ radiative decay of less than 2.3 times the predicted nominal rate for this process at the 90% confidence level (C.L.). The measurement disfavors a candidate photon interpretation of the MiniBooNE low-energy excess as a factor of 3.18 times the nominal NC Δ radiative decay rate at the 94.8% C.L., in favor of the nominal prediction, and represents a greater than 50-fold improvement over the world's best limit on single-photon production in NC interactions in the sub-GeV neutrino energy range.

DOI: 10.1103/PhysRevLett.128.111801

For over two decades, the anomalous signals consisting of MiniBooNE's low-energy excess (LEE) [1–3] and the prior LSND [4] $\bar{\nu}_e$ appearance results have been at the forefront of neutrino physics. Each has been interpreted as evidence for new types of neutrinos or other physics beyond the standard model (SM). The existence of new particles would be the first evidence for a new paradigm of physics associated with the neutrino sector since the discovery of neutrinos mass via their observed oscillations, and would have profound ramifications for all particle physics, astrophysics, and cosmology. At the heart of this puzzle of anomalies in need of interpretation is the fact MiniBooNE could not differentiate neutrino interactions producing an electron (such as from ν_e appearance due to light sterile neutrinos) from those with a single photon in the final state. Thus, both types of interactions must be examined independently as a source of the LEE.

Neutrino-induced neutral current (NC) production of the $\Delta(1232)$ baryon resonance with subsequent Δ radiative decay is predicted to be the dominant source of single photons in neutrino-argon scattering below 1 GeV [5]. Although Δ radiative decay is predicted in the SM, and measurements of photoproduction [6] and virtual compton scattering [7] are well described by theory, this process has never been directly observed in neutrino scattering. Previous searches have been performed by the T2K [8] and NOMAD [9] experiments with average incident neutrino energies E_ν of 0.85 and 25 GeV, respectively, resulting in leading limits on this process. Although on a different target, T2K's result is closest in E_ν to that of the MiniBooNE beam. However, the 90% confidence level (C.L.) limit is ~100 times the theoretically predicted rate of NC Δ radiative decay.

In this Letter, we present the world's most sensitive search for NC $\Delta \to N\gamma$, where $N = p, n$, using neutrino-argon scattering data collected by the MicroBooNE detector [10]. MicroBooNE is an 85 metric ton active volume liquid argon time projection chamber (LArTPC) situated at a similar baseline in the same muon neutrino dominated Booster Neutrino Beam (BNB) at Fermilab [11] as MiniBooNE, with $\langle E_\nu \rangle = 0.8$ GeV. The measurement

makes use of data corresponding to a BNB exposure of 6.80×10^{20} protons on target (POT), collected during 2016–2018. LArTPC technology allows MicroBooNE to distinguish electromagnetic showers originating from electrons or photons based on ionization energy deposition (dE/dx) at the start of the shower, and the nonzero conversion distance of the photon relative to the interaction vertex.

This search represents a first for this process with argon as the neutrino target, and also constitutes the first test of the MiniBooNE LEE under a single-photon interpretation. In a fit to the radial distribution of the MiniBooNE data with statistical errors only, an enhancement of NC $\Delta \to N\gamma$ (as predicted by the NUANCE [12] neutrino event generator on CH_2) by a normalization factor of $x_{\mathrm{MB}} = 3.18$ (quoted with no uncertainty) was found to provide the best fit for the observed LEE [3]. We perform an explicitly model-dependent test of this interpretation, cast as a factor of 3.18 enhancement to the predicted NC $\Delta \to N\gamma$ rate in MicroBooNE, under a two-hypothesis $\Delta\chi^2$ test between the enhanced rate and the nominal NC $\Delta \to N\gamma$ prediction.

MicroBooNE uses a custom tune [13] of the GENIE neutrino event generator v3.0.6 [14,15] to simulate neutrino-argon interactions. At BNB energies, the dominant source of single-photon production with no charged leptons or pions in the final state is NC $\Delta(1232) \to N\gamma$. This process is included in the MicroBooNE nominal prediction exactly as modeled in GENIE. Heavier resonances and nonresonant processes, including coherent single-photon production [16], are not currently included in the simulation, but are each estimated to contribute at the 10% level or less. Both these processes would produce slightly higher-energy photons than the $\Delta(1232)$ resonance, and a more forward (in the direction of the neutrino beam) photon in the case of coherent production. Although such events may be selected by this analysis, we do not explicitly quantify their selection efficiency and in this Letter we focus on the dominant NC $\Delta(1232) \to N\gamma$ process.

The MicroBooNE NC $\Delta \to N\gamma$ search exclusively targets events with a single, photonlike electromagnetic shower and either no other visible activity or one visible final-state proton. These are referred to as $1\gamma 0p$ and $1\gamma 1p$ events and primarily probe $\Delta \to n\gamma$ and $\Delta \to p\gamma$ decays, respectively. The analysis selects and simultaneously fits $1\gamma 1p$ and $1\gamma 0p$ data-to-Monte Carlo (MC) simulated distributions together with two additional, mutually exclusive but highly correlated event samples: $2\gamma 1p$, and $2\gamma 0p$. The signal, defined as all true NC $\Delta \to N\gamma$ events whose true interaction vertex is inside the active TPC, contributes predominantly to the 1γ event samples. The high-statistics 2γ samples are enhanced in NC $\Delta \to N\pi^0$ production, which is the dominant source of misidentified background to the $1\gamma 1p$ and $1\gamma 0p$ event samples.

Reconstruction of all four event samples makes use of the Pandora framework [17]. Reconstructed ionization charge hits are clustered and matched across three 2D projected views of the MicroBooNE active TPC volume into 3D reconstructed objects. These are then classified as tracks or showers based on a multivariate classifier score and aggregated into candidate neutrino interactions. The topological selection of interactions with exactly one shower and zero or one tracks represents the basis of the 1γ selections. Subsequently, preselection requires that the reconstructed vertex, shower-start point and track (as applicable) are all fully contained within the detector fiducial volume. A minimum energy requirement is imposed on the shower, ensuring good reconstruction performance, and a maximum track length requirement is imposed on the track, rejecting obvious muon backgrounds. Tracks are also required to have a high dE/dx consistent with that of a proton. Finally, an opening angle requirement between the track and shower directions is applied to eliminate colinear events where the start of a shower can be misreconstructed as a track.

The preselected events are fed into a set of boosted decision trees (BDTs), each designed to reject a distinct background and select NC $\Delta \to N\gamma$ events. The gradient boosting algorithm XGBoost [18] is used to train the BDTs. A cosmic BDT rejects cosmogenic backgrounds and is trained on cosmic ray data events collected when no neutrino beam was present. Track calorimetry is used to reject cosmic muons, with track and shower directionality-based variables proving powerful discriminators. A NC π^0 BDT compares the relationship of the reconstructed shower and track to those expected from π^0 decay kinematics to separate true single-photon events from those containing a π^0 decay where a second photon is not reconstructed. A charged current (CC) ν_e BDT targets the intrinsic ν_e background events. Here, the photon conversion distance and shower calorimetry play important roles. A fourth BDT is designed to veto events in which a second shower from a π^0 decay deposits some charge, but fails 3D shower reconstruction. Such events can result in 2D charge hits near the neutrino interaction that are not associated with a 3D object. A plane-by-plane clustering algorithm, DBSCAN [19], is used to group these unassociated hits, and properties including direction, shape, and energy of the cluster are used to determine consistency with a second shower from a π^0 decay. A final CC ν_μ-focused BDT removes any remaining backgrounds, primarily targeting the muon track through track calorimetry variables.

The $1\gamma 1p$ selection uses all five BDTs. The absence of a track in the $1\gamma 0p$ sample means that the $1\gamma 0p$ selection cannot use these BDTs identically, as it is limited to only shower variables. As such, it uses variations of the cosmic and NCπ^0 BDTs, and a third BDT merging the functionality of the CC ν_e and CC ν_μ-focused BDTs, targeting all remaining backgrounds. All BDTs are trained explicitly to select well-reconstructed NC $\Delta \to N\gamma$ events. While model dependent, this leverages the kinematics and correlations

TABLE I. Signal efficiencies for the $1\gamma 1p$ and $1\gamma 0p$ selections. The topological and combined efficiencies are evaluated relative to all true NC $\Delta \to N\gamma$ events inside the active TPC in the simulation (124.1 events expected for 6.80×10^{20} POT). The preselection and BDT selection efficiencies are evaluated relative to their respective preceding selection stage.

Selection stage	$1\gamma 1p$ eff.	$1\gamma 0p$ eff.
Topological	19.4%	13.5%
Preselection	63.9%	98.4%
BDT selection	32.1%	39.8%
Combined	3.99%	5.29%

between the track and shower associated with $\Delta(1232)$ resonance decay, particularly for the $1\gamma 1p$ selection. The BDTs for the $1\gamma 1p$ and $1\gamma 0p$ selections are trained and optimized for each selection independently, through a scan over grids of their BDT classifier scores. The optimized BDT classifier score cuts correspond to the highest statistical significance of the NC $\Delta \to N\gamma$ signal over background in each sample. The topological, preselection, BDT selection, and combined signal efficiencies are summarized in Table I.

The number of predicted background (both from simulation and cosmic ray data) events and NC $\Delta \to N\gamma$ signal events after BDT selection are summarized in Table II. A significant background to the search for single-photon events is NC π^0 events in which one of the decay photons is not reconstructed. This happens for a variety of reasons: (a) one of the photons from the π^0 decay may leave the detector active TPC volume before interacting, (b) the π^0 decay may be highly asymmetric leading to a secondary photon that is low in energy and not reconstructed, (c) both photons may be approximately colinear and overlapping and thus reconstructed as a single shower, or (d) the secondary photon may fall in a region of unresponsive wires, leading to poor reconstruction efficiency. Motivated by the background contribution of NC π^0 events, the $2\gamma 1p$ and $2\gamma 0p$ event samples serve to constrain the rate of NC π^0 background. The 2γ samples follow the same topological, preselection, and BDT selection scheme as the 1γ samples (see Supplemental Material [20]). The selected $2\gamma 1p$ and $2\gamma 0p$ events are shown in Fig. 1 as a function of reconstructed π^0 momentum, with a true NC $1\pi^0$ event purity of 63.4% and 59.6%, respectively. The data-to-MC simulation ratio in the $2\gamma 1p$ and $2\gamma 0p$ samples is $0.80 \pm 0.22(\text{stat} \oplus \text{syst})$ and $0.91 \pm 0.19(\text{stat} \oplus \text{syst})$, respectively, showing an overall deficit but one that is within 1σ.

TABLE II. The expected event rates in the $1\gamma 1p$ and $1\gamma 0p$ samples. "Dirt (outside TPC)" represents any neutrino interaction that originates outside the active TPC, but scatters inside. Relative to the topological selection stage, the ν_e CC rejection is 99.8% and 87.6% for $1\gamma 1p$ and $1\gamma 0p$, respectively.

Process	$1\gamma 1p$	$1\gamma 0p$
NC $1\pi^0$ Noncoherent	24.0	68.1
NC $1\pi^0$ Coherent	0.0	7.6
CC ν_μ $1\pi^0$	0.5	14.0
CC ν_e and $\bar{\nu}_e$	0.4	11.1
BNB other	2.1	18.1
Dirt (outside TPC)	0.0	36.4
Cosmic ray data	0.0	10.0
Total background (unconstr.)	27.0	165.4
NC $\Delta \to N\gamma$	4.88	6.55

The selected data and MC predictions are compared in a fit with a single free parameter corresponding to the normalization (x_Δ) of the nominal rate of NC $\Delta \to N\gamma$. A single bin is used for each of the $1\gamma 1p$ and $1\gamma 0p$ event samples, with reconstructed shower energy bin boundaries of 0–600 MeV and 100–700 MeV, respectively.

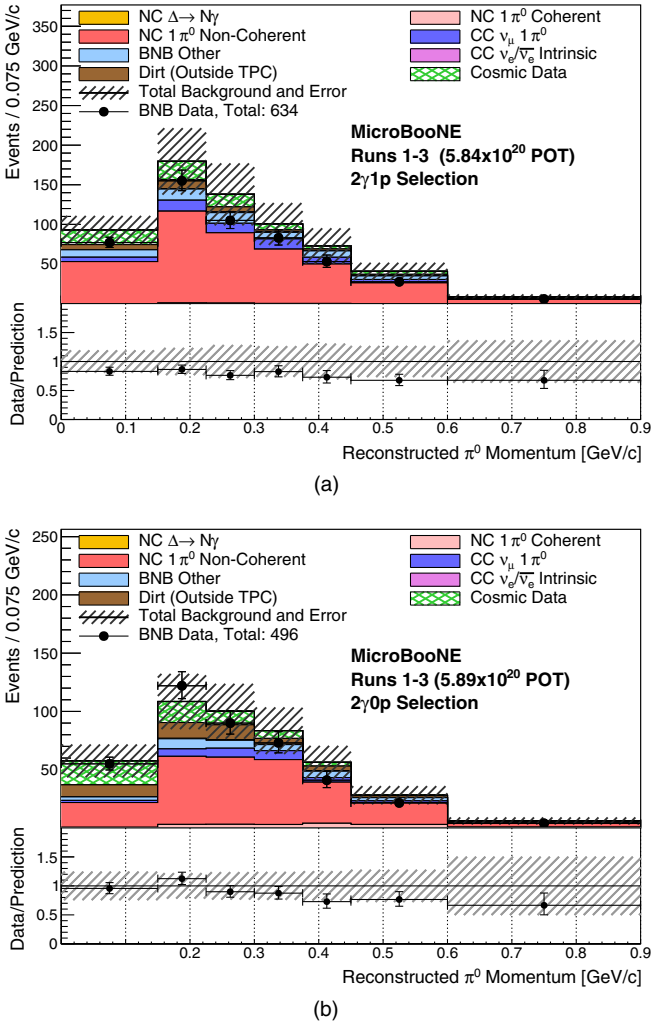

FIG. 1. Data and MC comparisons of the reconstructed π^0 momentum distributions for the (a) $2\gamma 1p$ and (b) $2\gamma 0p$ selected events.

The one-bin $1\gamma 1p$ and $1\gamma 0p$ event rates are fit simultaneously with the $2\gamma 1p$ and $2\gamma 0p$ distributions shown in Fig. 1. The fit makes use of a covariance matrix that encapsulates statistical and systematic uncertainties and bin-to-bin correlations, allowing for both the expected rate and uncertainties of the NC π^0 backgrounds in the 1γ samples to be effectively constrained by the high-statistics data observed in the 2γ samples.

The normalization x_Δ can also be reinterpreted in various ways. First, it can be reinterpreted as a scaling of an effective branching fraction $\mathcal{B}_{\text{eff}}(\Delta \to N\gamma)$, where the nominal prediction ($x_\Delta = 1$) corresponds to an effective branching fraction of 0.6%. This effective branching fraction can be thought of as a metric to account for any uncertain nuclear effects that might modify the Δ behavior inside the nuclear medium, as we cannot observe the true $\Delta \to N\gamma$ branching fraction directly. In addition, any BSM effect that can contribute as an NC Δ-like process (with a single photonlike shower in the final state) could lead to an effective modification to the observed branching fraction. Although GENIE prescribes a normalization uncertainty for $\mathcal{B}_{\text{eff}}(\Delta \to N\gamma)$, this uncertainty is not included in the fit. In addition, with the knowledge that GENIE predicts a cross section for NC $\Delta \to N\gamma$ production to be $\sigma^{\text{GENIE,Ar}}_{NC\Delta\to N\gamma} = 8.61 \times 10^{-42}$ cm^{-2}/nucleon, we can also reinterpret x_Δ as scaling on this production cross section. The Feldman-Cousins [21] approach is followed to construct the confidence intervals for x_Δ given the best fit to the observed data, with a metric of $\Delta\chi^2$ defined using the combined-Neyman-Pearson χ^2 [22] as an approximation of the log-likelihood ratio.

Systematic uncertainties include contributions from flux, cross-section modeling, hadron reinteractions, detector effects, and finite statistics used in the background predictions (both MC and cosmic ray data). The flux uncertainties incorporate hadron production uncertainties, uncertainties on pion and nucleon scattering in the beryllium target and surrounding aluminum magnetic horn, and mis-modeling of the horn current. Following Ref. [23], these are implemented by reweighting the flux prediction and studying the propagated effects on event distributions. The cross-section uncertainties incorporate modeling uncertainties on the GENIE prediction [13,15,24], evaluated also by reweighting tools. The hadron-argon reinteraction uncertainties are associated with the propagation of hadrons through the detector, as modeled in GEANT4 [25]. The detector modeling and response uncertainties are evaluated using a novel data-driven technique. This uses *in situ* measurements of distortions in the TPC wire readout signals due to various detector effects, such as diffusion, electron drift lifetime, electric field, and electronics response, to parametrize these effects at the TPC wire level, and provides a detector model-agnostic way to study and evaluate their effects on event distributions [26]. Additional systematics varying the charge recombination model, the scintillation light yield, and space charge effects [27,28] are separately included. The uncertainty on photonuclear absorption of photons on argon was evaluated to be at the subpercent level, and is therefore omitted. There is also no assigned uncertainty for heavier resonances or coherent single-photon production, which are not simulated in GENIE. Finally, an inconsistency was identified in the GENIE v3.0.6 reweighing code used to evaluate a small subset of systematic uncertainties, but was found to have negligible impact on the analysis sensitivity and thus has been ignored.

TABLE III. Breakdown of background systematic uncertainties for the $1\gamma 1p$ and $1\gamma 0p$ samples.

Type of uncertainty	$1\gamma 1p$	$1\gamma 0p$
Flux model	7.4%	6.6%
GENIE cross-section model	24.8%	16.3%
GEANT4 reinteractions	1.1%	1.3%
Detector effects	12.2%	6.4%
Finite background statistics	8.3%	4.0%
Total uncertainty (unconstr.)	29.8%	19.2%
Total uncertainty (constr.)	17.8%	9.5%

The fractional systematic uncertainties on the $1\gamma 1p$ and $1\gamma 0p$ total background events are summarized in Table III. The GENIE cross-section uncertainties dominate. This stems from the uncertainties on NC π^0 production on argon, which forms the largest background and has not been measured to high precision to date. Both cross-section and flux uncertainties are strongly correlated between the 1γ and 2γ event samples. The simultaneous fit to the 1γ and 2γ samples is equivalent to a 1γ-only fit where the background and uncertainty are conditionally constrained [29] by the 2γ samples. Given the 2γ samples' statistics, this constraint effectively reduces the total background systematic uncertainty of the $1\gamma 1p$ and $1\gamma 0p$ samples by 40% and 50%, and the total background prediction by 24.1% and 12.3%, respectively.

The 90% C.L. sensitivity is quantified for a Feldman-Cousins-corrected limit in the case of a background-only observation, $x_\Delta = 0$, to be less than $x_\Delta = 2.5$, corresponding to $\mathcal{B}_{\text{eff}}(\Delta \to N\gamma) = 1.50\%$ and $\sigma^{\text{Ar}}_{NC\Delta\to N\gamma} = 21.5 \times 10^{-42}$ cm^{-2}/nucleon. Under a two-hypothesis $\Delta\chi^2$ test, the expected sensitivity of the median experiment assuming the nominal prediction, to reject the LEE hypothesis ($x_{\text{MB}} = 3.18$) in favor of the nominal hypothesis ($x_\Delta = 1$) is 1.5σ; in the case of the median experiment assuming the LEE hypothesis, the sensitivity to reject the nominal hypothesis in favor of the LEE hypothesis is 1.6σ.

The reconstruction, selection, and fitting methods employed in this search were developed adhering to a signal-blind analysis strategy, whereby the data were kept blind until the analysis was fully developed, with the

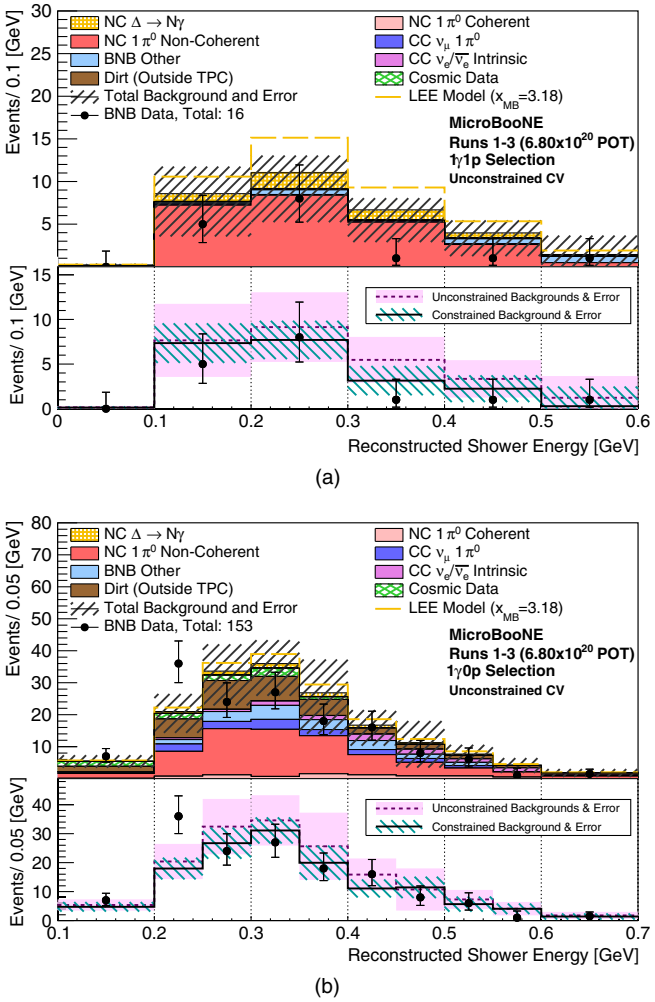

FIG. 2. Energy spectra for the (a) $1\gamma 1p$ and (b) $1\gamma 0p$ selected events. The upper section in each figure shows the unconstrained background predictions and breakdowns as a function of reconstructed shower energy. The lower section shows the total background prediction with systematic uncertainty both before and after the 2γ constraint. The local significance of the data fluctuation in the 200–250 MeV bin of (b) corresponds to 1.6σ ($\chi^2/\text{d.o.f.} = 3.66/1$) before the 2γ constraint, and 2.7σ ($\chi^2/\text{d.o.f.} = 8.54/1$) after. From MC studies, the probability of any one bin across all 16 1γ bins giving rise to a constrained $\chi^2 \geq 8.54$ is 4.74%.

exception of a small subset of the data consisting of 0.51×10^{20} POT, used for analysis validation. After $1\gamma 1p$ and $1\gamma 0p$ event samples were unblinded, 16 data events with an expected constrained background of $20.5 \pm 3.6(\text{syst})$ events were observed in the $1\gamma 1p$ event sample, and 153 data events with an expected constrained background of $145.1 \pm 13.8(\text{syst})$ events were observed in the $1\gamma 0p$ event sample. The reconstructed shower energy distributions of selected $1\gamma 1p$ and $1\gamma 0p$ events are shown in Fig. 2. Overall, a systematic deficit of data relative to the unconstrained MC prediction is observed, which is within systematic and statistical uncertainties, and consistent with a similar deficit

TABLE IV. Number of predicted background, predicted signal, and observed data events for the $1\gamma 1p$ and $1\gamma 0p$ samples, with background systematic uncertainties.

	$1\gamma 1p$	$1\gamma 0p$
Unconstr. bkgd.	27.0 ± 8.1	165.4 ± 31.7
Constr. bkgd.	20.5 ± 3.6	145.1 ± 13.8
NC $\Delta \to N\gamma$	4.88	6.55
LEE ($x_{\text{MB}} = 3.18$)	15.5	20.1
Data	16	153

in the 2γ event samples. The expected signal and background predictions are summarized in Table IV and Fig. 3, and compared to the observed data, both before and after applying the 2γ conditional constraint. The 2γ constraint reduces the total background prediction, consistently with

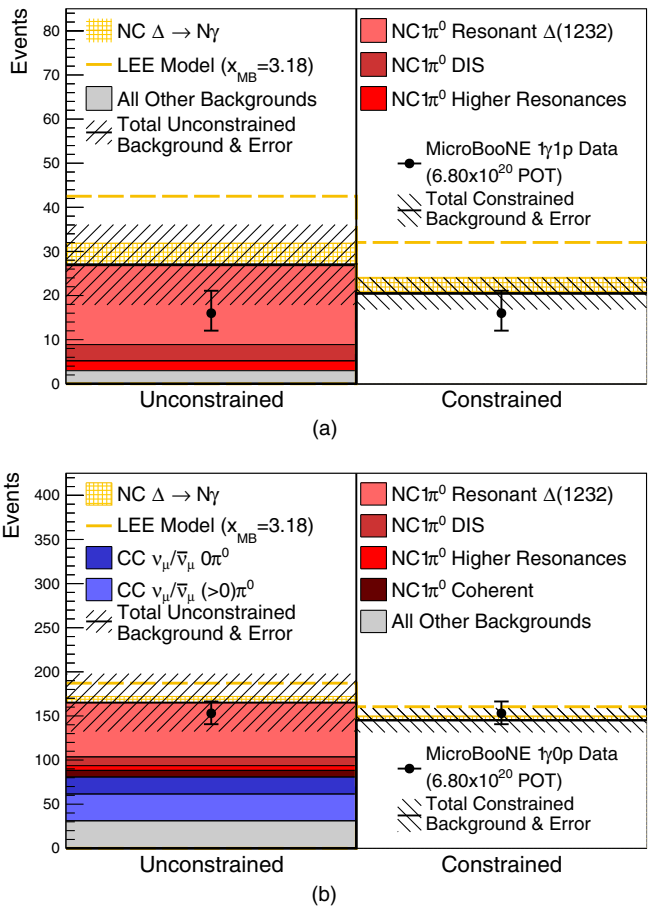

FIG. 3. The observed event rates for the (a) $1\gamma 1p$ and (b) $1\gamma 0p$ event samples, and comparisons to unconstrained (left) and constrained (right) background and LEE model predictions. The event rates are the sum of all events with reconstructed shower energy between 0–600 MeV and 100–700 MeV for (a) and (b), respectively. The one-bin background only conditionally constrained χ^2 is 0.63 and 0.18 for $1\gamma 1p$ and $1\gamma 0p$, respectively.

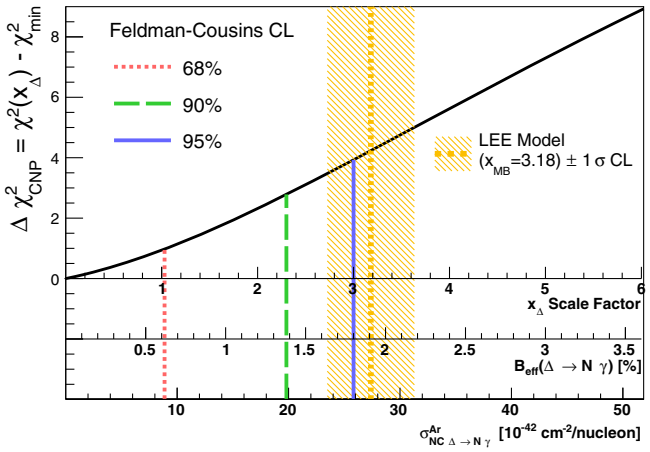

FIG. 4. The resulting $\Delta\chi^2$ curve after fitting to x_Δ using the Feldman-Cousins procedure, showing extracted confidence intervals. The best fit is found to be at $x_\Delta = 0$ with a $\chi^2_{\rm bf} = 5.53$. Shown also is the reinterpretation of this scaling factor as both an effective branching fraction, $\mathcal{B}_{\rm eff}(\Delta \to N\gamma)$, and a cross section, $\sigma^{\rm Ar}_{{\rm NC}\Delta\to N\gamma}$. The default GENIE value corresponds to $x_\Delta = 1$. The error on the LEE model is estimated from the MiniBooNE result [3] with statistical and systematic uncertainty. It should be noted that this uncertainty does not account for systematic correlations between MiniBooNE and MicroBooNE.

the data to MC simulation ratio observed in the 2γ event samples.

The best-fit value for x_Δ obtained from the fit is 0, with a χ^2_{bf} of 5.53 for 15 degrees of freedom (d.o.f.). This measurement is in agreement with the nominal NC $\Delta \to N\gamma$ rate (corresponding to $x_\Delta = 1$) within 1σ (67.8% C.L.) with a χ^2 of 6.47 for 16 d.o.f. The Feldman-Cousins calculated confidence limit leads to a one-sided bound on the normalization of NC $\Delta \to N\gamma$ events of $x_\Delta < 2.3$, corresponding to $\mathcal{B}_{\rm eff}(\Delta \to N\gamma) < 1.38\%$ and $\sigma^{\rm Ar}_{{\rm NC}\Delta\to N\gamma} < 19.8 \times 10^{-42}$ cm^{-2}/nucleon, at 90% C.L. This is summarized in Fig. 4.

This result represents the most stringent limit on neutrino-induced NC $\Delta \to N\gamma$ on any nuclear target [8,9], and a significant improvement over previous searches, in particular in the neutrino energy range below 1 GeV. Under a two-hypothesis test, the data rule out the interpretation of the MiniBooNE anomalous excess [30] as a factor of 3.18 enhancement to the rate of $\Delta \to N\gamma$, in favor of the nominal prediction at 94.8% C.L. (1.9σ). While this is a model-dependent test of the MiniBooNE LEE, and does not apply universally to all other photonlike interpretations, it provides an important constraint on this process and a first direct test of the MiniBooNE LEE, and opens the door to further searches that focus on a broader range of models. Those include coherent single-photon production [5], anomalous contributions of which could give rise to additional events and would be expected to leave an imprint in the $1\gamma 0p$ selection, as well as more exotic beyond-SM processes that manifest as single-photon events, such as colinear e^+e^- pairs from Z' [31,32] or scalar [33] decays, among others. Follow-up MicroBooNE analyses will explicitly target and quantify sensitivity to these alternative hypotheses, as well as model-independent single-photon searches.

This document was prepared by the MicroBooNE Collaboration using the resources of the Fermi National Accelerator Laboratory (Fermilab), a U.S. Department of Energy, Office of Science, HEP User Facility. Fermilab is managed by Fermi Research Alliance, LLC (FRA), acting under Contract No. DE-AC02-07CH11359. MicroBooNE is supported by the U.S. Department of Energy, Office of Science, Offices of High Energy Physics and Nuclear Physics; the U.S. National Science Foundation; the Swiss National Science Foundation; the Science and Technology Facilities Council (STFC), part of the United Kingdom Research and Innovation; the Royal Society (United Kingdom); and The European Union's Horizon 2020 Marie Skłodowska-Curie Actions. Additional support for the laser calibration system and cosmic ray tagger was provided by the Albert Einstein Center for Fundamental Physics, Bern, Switzerland.

*microboone_info@fnal.gov

[1] A. A. Aguilar-Arevalo *et al.* (MiniBooNE Collaboration), Phys. Rev. Lett. **102**, 101802 (2009).
[2] A. A. Aguilar-Arevalo *et al.* (MiniBooNE Collaboration), Phys. Rev. Lett. **121**, 221801 (2018).
[3] A. A. Aguilar-Arevalo *et al.* (MiniBooNE Collaboration), Phys. Rev. D **103**, 052002 (2021).
[4] C. Athanassopoulos *et al.* (LSND Collaboration), Phys. Rev. C **54**, 2685 (1996).
[5] E. Wang, L. Alvarez-Ruso, and J. Nieves, Phys. Rev. C **89**, 015503 (2014).
[6] G. Blanpied *et al.*, Phys. Rev. Lett. **79**, 4337 (1997).
[7] N. F. Sparveris *et al.*, Phys. Rev. C **78**, 018201 (2008).
[8] K. Abe *et al.* (T2K Collaboration), J. Phys. G **46**, 08LT01 (2019).
[9] C. Kullenberg *et al.* (NOMAD Collaboration), Phys. Lett. B **706**, 268 (2012).
[10] R. Acciarri *et al.* (MicroBooNE Collaboration), J. Instrum. **12**, P02017 (2017).
[11] A. A. Aguilar-Arevalo *et al.* (MiniBooNE Collaboration), Phys. Rev. D **79**, 072002 (2009).
[12] D. Casper, Nucl. Phys. B, Proc. Suppl. **112**, 161 (2002).
[13] P. Abratenko *et al.* (MicroBooNE Collaboration), arXiv: 2110.14028.
[14] C. Andreopoulos *et al.*, Nucl. Instrum. Methods Phys. Res., Sect. A **614**, 87 (2010).
[15] J. Tena-Vidal *et al.* (GENIE Collaboration), Phys. Rev. D **104**, 072009 (2021).
[16] L. Alvarez-Ruso, J. Nieves, E. Sala, and E. Wang, J. Phys. Conf. Ser. **1056**, 012001 (2018).
[17] R. Acciarri *et al.* (MicroBooNE Collaboration), Eur. Phys. J. C **78**, 82 (2018).

[18] T. Chen and C. Guestrin, *Proceedings of the 22nd ACM SIGKDD International Conference on Knowledge Discovery and Data Mining* (Association for Computing Machinery, New York, USA, 2016), pp. 785–794.
[19] M. Ester *et al.*, *KDD'96: Proceedings of the Second International Conference on Knowledge Discovery and Data Mining* (AAAI Press, Portland, Oregon, 1996), pp. 226–231.
[20] See Supplemental Material at http://link.aps.org/supplemental/10.1103/PhysRevLett.128.111801 for a description of the two shower NCπ^0 rich selections as well as a data release corresponding to the results shown in this paper.
[21] G. J. Feldman and R. D. Cousins, Phys. Rev. D **57**, 3873 (1998).
[22] X. Ji, W. Gu, X. Qian, H. Wei, and C. Zhang, Nucl. Instrum. Methods Phys. Res., Sect. A **961**, 163677 (2020).
[23] P. Abratenko *et al.* (MicroBooNE Collaboration), Phys. Rev. Lett. **123**, 131801 (2019).
[24] C. Andreopoulos *et al.*, Nucl. Instrum. Methods Phys. Res., Sect. A **614**, 87 (2010).
[25] S. Agostinelli *et al.*, Nucl. Instrum. Methods Phys. Res., Sect. A **506**, 250 (2003).
[26] P. Abratenko *et al.* (MicroBooNE Collaboration), arXiv:2111.03556.
[27] P. Abratenko *et al.* (MicroBooNE Collaboration), J. Instrum. **15**, P07010 (2020).
[28] P. Abratenko *et al.* (MicroBooNE Collaboration), J. Instrum. **15**, P12037 (2020).
[29] M. L. Eaton, *Multivariate Statistics: A Vector Space Approach*, Wiley series in probability and mathematical statistics. Probability and mathematical statistics (Wiley, New York, 1983–1983).
[30] A. Aguilar-Arevalo *et al.* (MiniBooNE Collaboration), Phys. Rev. Lett. **102**, 101802 (2009).
[31] E. Bertuzzo, S. Jana, P. A. N. Machado, and R. Z. Funchal, Phys. Rev. Lett. **121**, 241801 (2018).
[32] P. Ballett, S. Pascoli, and M. Ross-Lonergan, Phys. Rev. D **99**, 071701(R) (2019).
[33] W. Abdallah, R. Gandhi, and S. Roy, Phys. Rev. D **104**, 055028 (2021).